Supporting Information

Innocuous solvent-based, low-temperature curable, and high transparency photosensitive polyimides developed by soluble polyimides containing bio-based magnolol moieties

Huifa Meng[a, b], *Kaijin Chen*[b], *Chuying Li*[b], *Longfei Zhang*[c], *Yanwei He*[d], *Zining Zhao*[b], *Peixin Wu*[b], *Hai Zhu*[c], *Zhenguo Chi*[e], *Jiarui Xu*[b], *Siwei Liu*[b], *and Yi Zhang*[a, b, *]

[a]School of Chemical Engineering and Technology, GBRCE for Functional Molecular Engineering, IGCME, Sun Yat-sen University, 519082 Zhuhai, China.

[b]PCFM Lab, GD HPPC Lab, Guangdong Engineering Technology Research Centre for High-performance Organic and Polymer Photoelectric Functional Films, State Key Laboratory of Optoelectronic Materials and Technologies, School of Chemistry, Sun Yat-sen University, Guangzhou 510275, China.

[c]School of Physics, Sun Yat-sen University, Guangzhou 510275, China.

[d]Wuxi Shunxuan New Materials Co., Ltd., Wuxi 214037, China.

[e]School of Environmental and Chemical Engineering, Wuyi University, Jiangmen, 529020, China.

E-mail: ceszy@mail.sysu.edu.cn(*Yi Zhang*)

Contents

Experimental Section

Synthesis of 5,5'-diallyl-[1,1'-biphenyl]-2,2'-diyl bis(4-bromobenzoate) (DDBr)

To a 500 mL three-neck flask equipped with a magnetic stirrer, an argon inlet and a dropping funnel, 4-bromobenzoyl chloride (24.14 g, 105 mmol) was dissolved in 120mL tetrahydrofuran (THF) and the mixture was cooled and kept at 0 °C. Then a THF solution (60 mL) of magnolol (13.32 g, 50 mmol) and TEA (20.9 mL,150mmol) was added dropwise over 1 h. After stirring for 12 h at room temperature, the solution was extracted by dilute hydrochloric acid and deionized water to neutralization. Subsequently, the organic layer was dried and purified by silica-gel column chromatography (petroleum ether/DCM, 3/1, V/V) to give the white powders in the yield of 92.1%. ^{1}H NMR (400 MHz, Chloroform-*d*) *δ*: 7.78 (dt, J = 8.8, 2.3 Hz, 2H), 7.54 (dt, J = 8.9, 2.3 Hz, 2H), 7.18 (d, J = 1.9 Hz, 3H), 5.82 (ddt, J = 17.6, 9.5, 6.7 Hz, 1H), 4.99 (dq, J = 13.1, 1.8 Hz, 2H), 3.33 (dt, J = 6.6, 1.7 Hz, 2H). ^{13}C NMR (151 MHz, Chloroform-*d*) *δ*: 164.44, 146.52, 137.92, 136.93, 131.91, 131.65, 131.33, 130.27, 129.33, 128.76, 128.47, 122.54, 116.31, 39.61. HR-MS (ESI, m/z): $[M+Na]^+$ calcd for $C_{32}H_{24}Br_2O_4Na$, 654.99131, found 654.99156.

Synthesis of 5,5'-diallyl-[1,1'-biphenyl]-2,2'-diyl bis(4'-amino-[1,1'-biphenyl]-4-carboxylate) (DDBA)

DDBr (9.48 g, 15 mmol) and $Pd(PPh_3)_4$ (catalytic amount) were dissolved in 250 mL tetrahydrofuran (THF) under the argon condition. After stirring for 10 min, 3 M aqueous K_3PO_4 solution (60 mL) was added. Then (4-aminophenyl)boronic acid hydrochloride (7.80 g, 45 mmol) was added and the mixture was further stirred at 75 °C for 24 h. After cooling to room temperature, the crude products were concentrated and purified by silica-gel column chromatography (petroleum ether/DCM, 1/4, V/V) to give the yellow powders in the yield of 88.1%. ^{1}H NMR (400 MHz, DMSO-d_6) *δ*: 7.89 (d, J = 8.3 Hz, 2H), 7.69 (d, J = 8.4 Hz, 2H), 7.48 (d, J = 8.4 Hz, 2H), 7.32 – 7.13 (m, 3H), 6.66 (d, J = 8.5 Hz, 2H), 5.89 – 5.73 (m, 1H), 5.45 (s, 2H), 5.09 – 4.85 (m, 2H), 3.34 (s, 4H). ^{13}C NMR (151 MHz, DMSO-d_6) *δ*: 164.32, 149.63, 146.21, 145.79, 137.29, 137.19, 130.76, 130.23, 129.83, 129.07, 127.71, 125.42, 125.25, 125.02, 123.00, 116.05, 114.14, 38.65. HR-MS (ESI, m/z): $[M+H]^+$ calcd for $C_{44}H_{37}N_2O_4$,

657.27478, found 657.27442.

Characterization

Structural characterization

^{1}H NMR and ^{13}C NMR spectra were recorded on a Bruker AVANCE 400 or 600 spectrometer using deuterated chloroform ($CDCl_3$) or deuterated dimethyl sulfoxide (DMSO-d_6) as the solvent. High resolution mass spectra (HR-MS) were carried out on a high resolution orbitrap liquid chromatograph-mass spectrometer (Q Exactive, Thermo Scientific, Germany).

Spectral characterization

Fourier transform infrared (FT-IR) spectra were obtained on a Nicolet iS50 spectrometer in the fundamental wavenumber ranges of 500~4000 cm^{-1}. Absorption spectra were obtained using a Hitachi UV-Vis spectrophotometer (U-3900) in the range of 200-800 nm.

Molecular weight, intrinsic viscosities, and WAXD characterization

Gel permeation chromatography (GPC) was conducted against polymethyl methacrylate internal standard of known molecular weight on a Waters Model 717 plus autosampler with a Waters Model 1515 isocratic HPLC pump, using DMF with 0.05M LiBr as the eluent solvents at a flow rate of 1.0 mL min^{-1}. The intrinsic viscosities (η) of the soluble polyimides were measured on an Ubbelohde viscometer in 0.5 dL/g PI solutions in PGEMA at 30 °C. Wide-angle X-ray diffraction (WAXD) was carried out on an X-ray diffractometer (Rigaku Smart Lab).

Chemical resistance

Cured films was dipped in various solvents, *N*-methyl pyrrolidone (NMP), 2-acetoxy-1-methoxypropane (PGEMA), acetone, 30% nitric acid aq., 30% sulfuric acid aq., and hydrogen peroxide (H_2O_2), at 24 ◦C for 15 min, and then measured the change in film thickness.

Mechanical, thermal properties

Mechanical properties and glass transition temperature of PI films carried out on a DMA Q800 analyzer (TA Company, USA), in which the tensile test was measured at the displacement rate of 10 μm min^{-1} and the thermal performance test was performed

at a heating rate of 3 °C min^{-1} and a constant frequency of 1 Hz. The coefficient of thermal expansion (CTE) is the amount by which a material expands when heated below its glass transition temperature, which values were measured using a static mechanical analyzer (Q400 from TA Instruments) at a heating rate of 10 °C min^{-1}. Thermogravimetric analysis (TGA) was performed on a thermal gravimetric analyzer (PE Pyris1 TGA) at a heating rate of 10 °C min^{-1} under nitrogen flow of 20 mL min^{-1}. Thermogravimetry-infrared analysis (TG-IR) was performed on a STA 449F3 simultaneous thermal analyzer combined with a Nicolet 6700 spectrometer.

To be qualitative, the cross-linking density (ve) of cured PI films can be calculated using the kinetic theory of rubber elasticity equation[1]:

$$Er = 6veRT$$

where Er is the storage modulus at T = (T_g + 40) absolute temperature, R is the gas constant (8.314 $J \cdot K^{-1} \cdot mol^{-1}$) and T_g is determined by the maximum tan delta value.

Water adsorption, dielectric, and breakdown strength properties

The adsorption isotherms of ‘‘the gravimetric method’’ were conducted on a Vacuum & Dynamic Vapor/Gas Sorption equipment (Beishide Instrument Technology (Beijing) Co., Ltd). The high frequency dielectric properties of the PI films were performed using a network analyzer P5003A (Keysight Technologies, America) with a cavity resonator of 10 GHz (QWED, Poland). Dielectric breakdown strength of PI films was measured for 10 samples using a CS9915AX Programmable AC withstand Voltage Tester with a maximum voltage of 10 kV, at approximately 500 V/s until the point of failure. The measurements were carried out at room temperature in silicone oil.

Weibull characteristic breakdown strength of cured PI films was then investigated at room temperature. The electric breakdown strength of the polymers was analyzed by a two-parameter Weibull distribution function[2]:

$$P(E) = 1 - exp\left[\frac{E}{E_b}\right]^{\beta}$$

where *P(E)* represents the probability of breakdown, E is the experimental electrical breakdown field, E_b represents the Weibull breakdown strength at 63.2% probability of breakdown, β is the shape parameter utilized to evaluate the scatter of experimental

data.

Lithographic properties

The lithographic patterns of PI photoresist were performed on a maskless lithography machine (uPG501, Heidelberg), using 380 nm light and a micro-mirror array. The lithographic performance of PSPIs was performed on a field emission scanning electron microscope (SEM, Hitachi S-4800) equipped an Energy Dispersive Spectrometer (EDS) and a digital microscope (DSX10-SZH, Olympus). AFM images were recorded using a Bruker Multimode 8 (Bruker, USA) instrument operated in the scanasyst mode under ambient conditions.

Theoretical calculation

The planarity of the molecule was quantified and graphically investigated using Multiwfn[3]. The optimized molecular structures were obtained at B3LYP-D3(BJ)/6-31G(d) level by using the Gaussian 16 program[4]. The time-dependent density functional theory (TD-DFT) calculation was performed at the B3LYP-D3(BJ), 6-31G(d) basis set on the geometries optimized oligomers. Excitation energies and oscillator strengths were calculated from the ground state to ten excited states, with each transition broadened using a Gaussian function that incorporated the above quantities. Ultimately, the afore-mentioned leaps were superimposed to generate the simulated UV-Vis absorption curves. The Molecular Dynamics (MD) simulation was constructed by randomly placing 10 polymer chains with 30 repeating units in a cubic box base on Gromacs 2024.2 simulation package[5]. In the course of the simulation, periodic boundary conditions were applied, and the system was balanced using both the canonical ensemble (NVT) and the constant-pressure, constant-temperature (NPT) ensembles in a flexible manner. The aforementioned process entailed the control of pressure through the C-rescale method and temperature through the velocity rescaling method. Subsequent to the system's balancing, a 20 ns simulation was conducted under the NVT ensemble to obtain data. The radial distribution functions (RDF) were generated using gmx rdf.

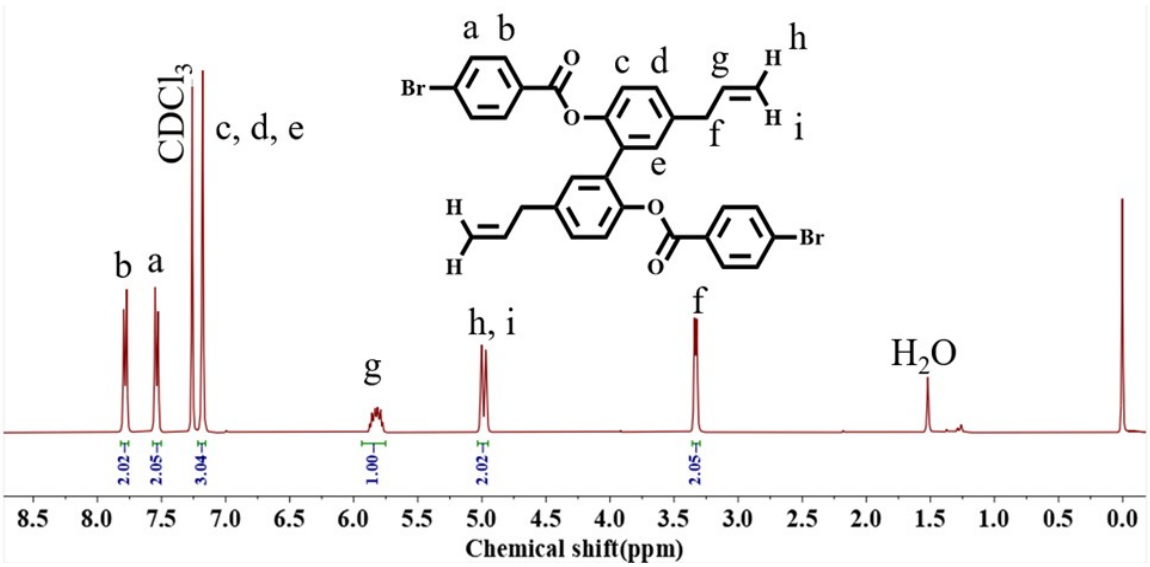

Fig. S1. ^{1}H NMR spectrum of DDBr in $CDCl_3$.

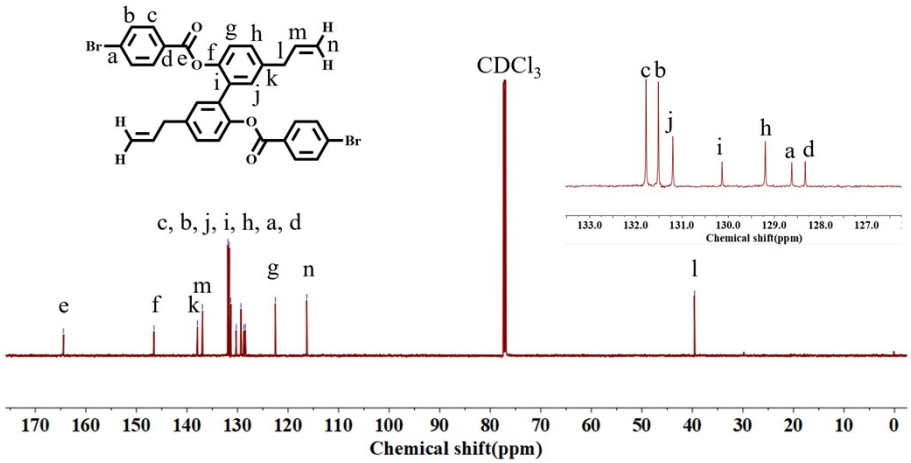

Fig. S2. ^{13}C NMR spectrum of DDBr in $CDCl_3$.

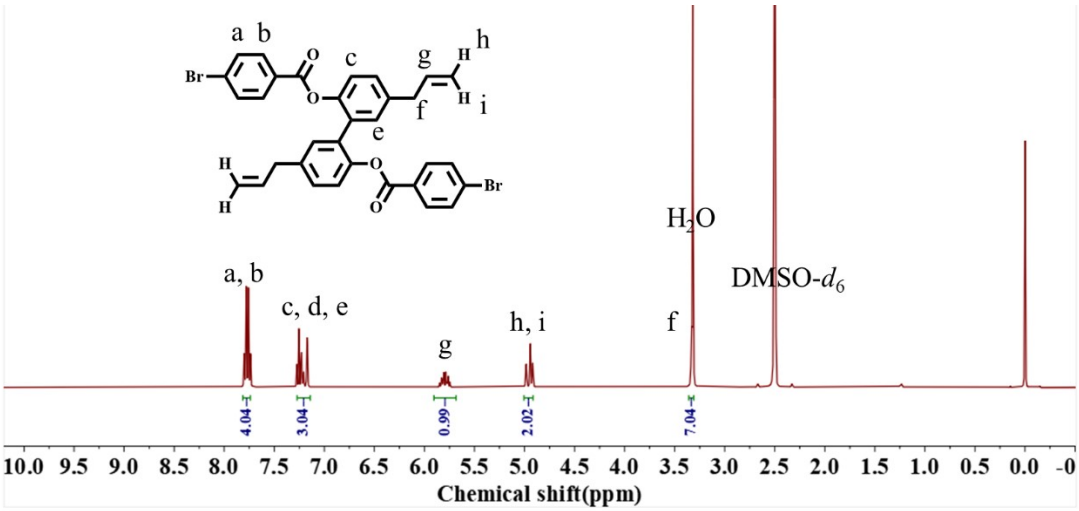

Fig. S3. ^{1}H NMR spectrum of DDBr in DMSO-d_6.

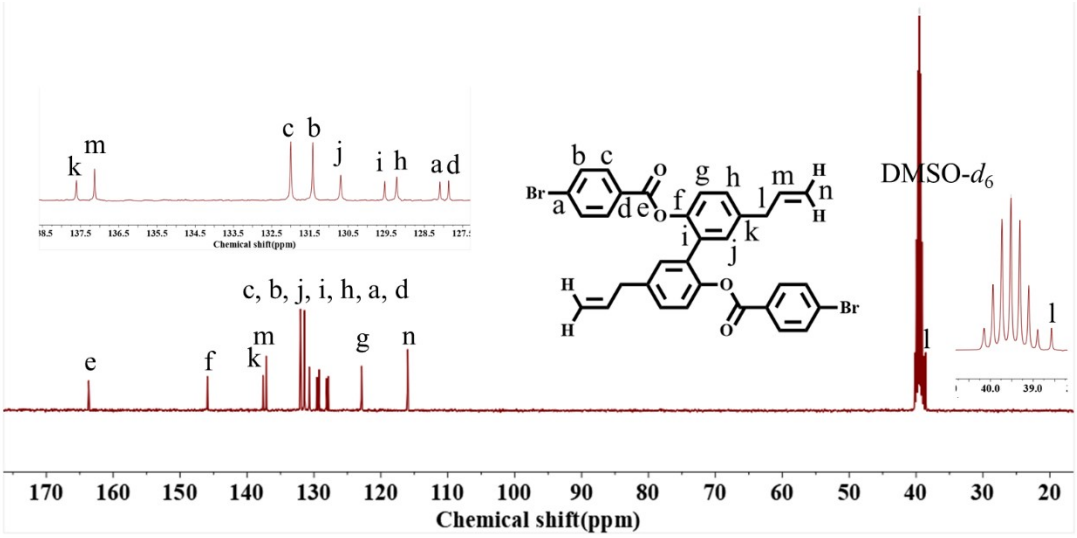

Fig. S4. ^{13}C NMR spectrum of DDBr in DMSO-d_6.

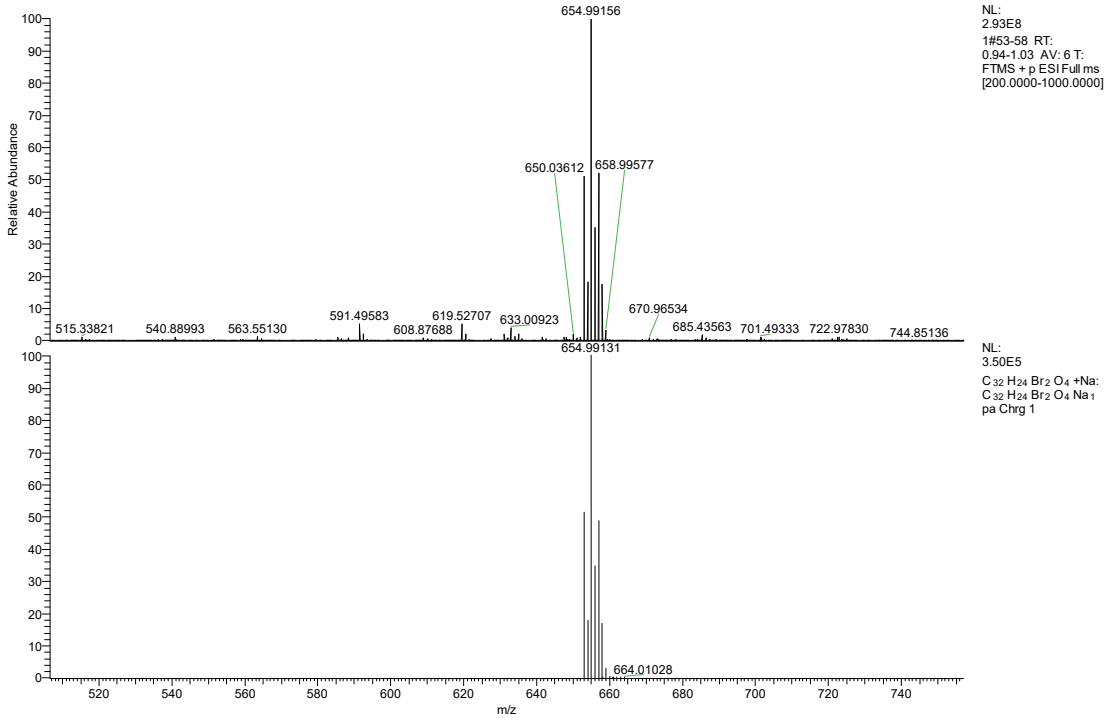

Fig. S5. ESI-MS spectrum of DDBr at room temperature.

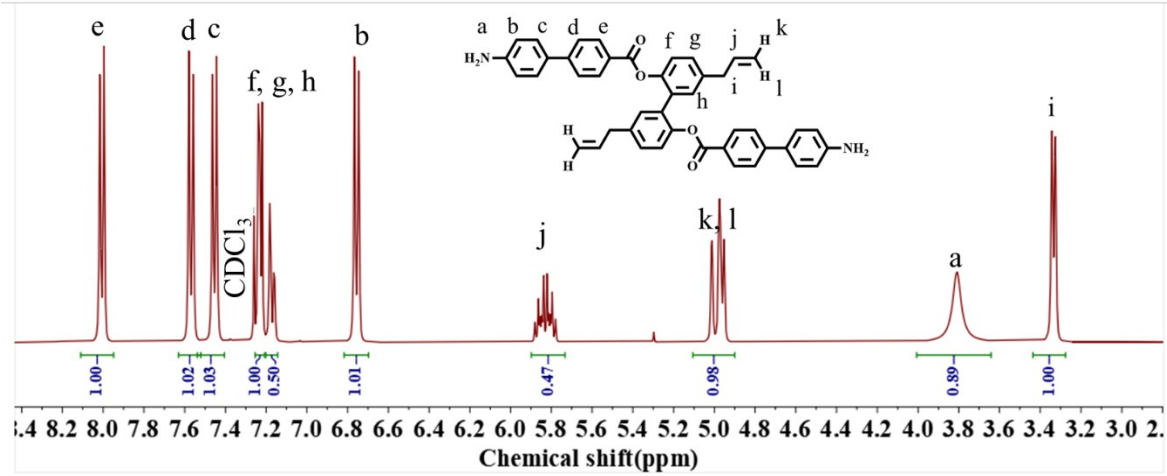

Fig. S6. ^{1}H NMR spectrum of DDBA in $CDCl_3$.

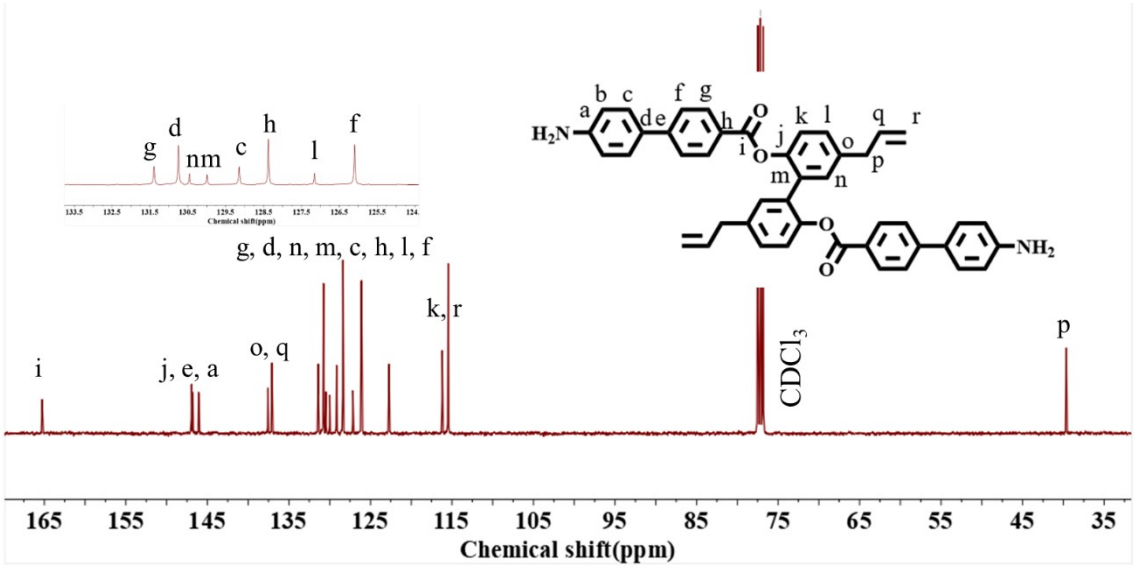

Fig. S7. ^{13}C NMR spectrum of DDBA in $CDCl_3$.

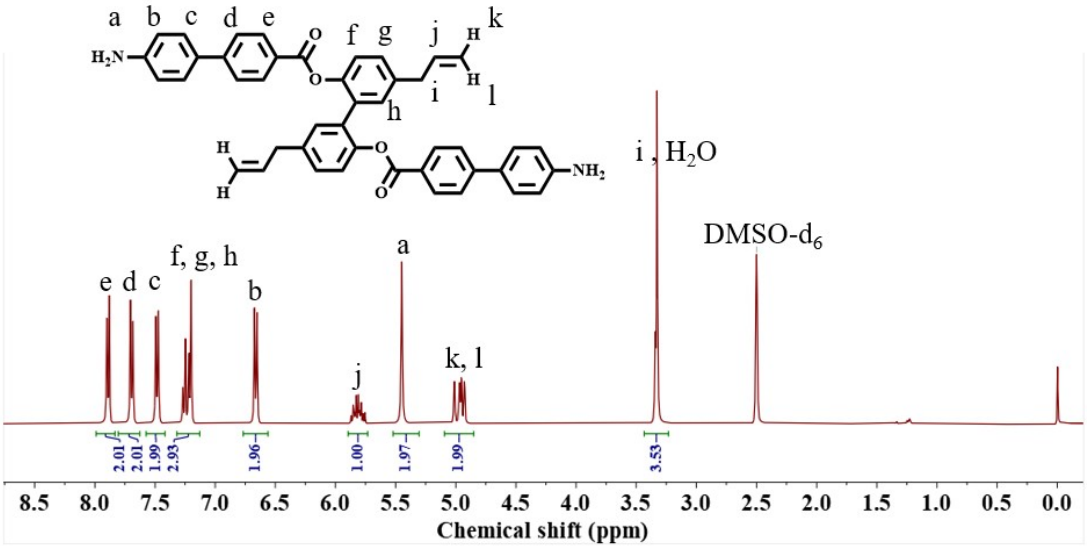

Fig. S8. ^{1}H NMR spectrum of DDBA in DMSO-d_6.

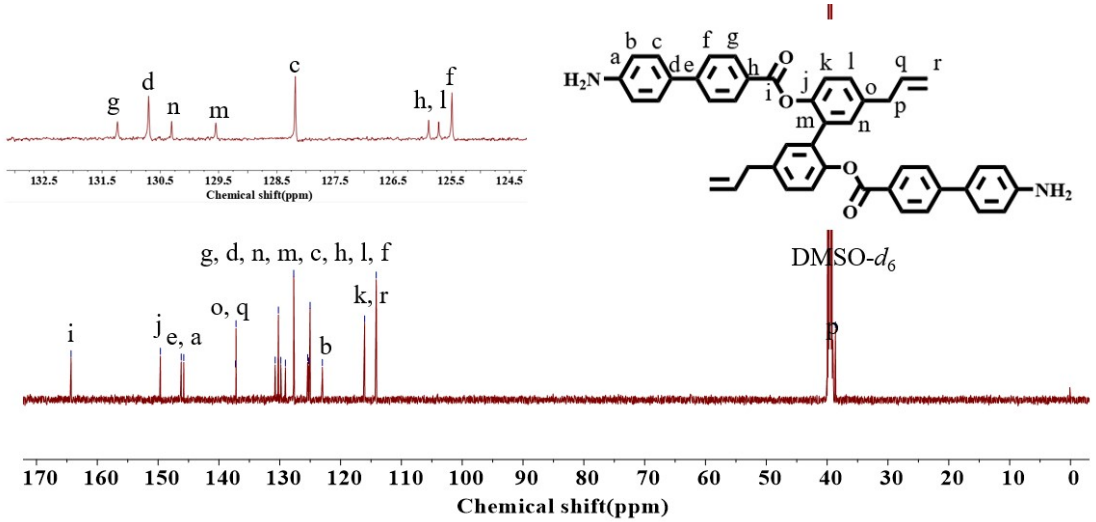

Fig. S9. ^{13}C NMR spectrum of DDBA in DMSO-d_6.

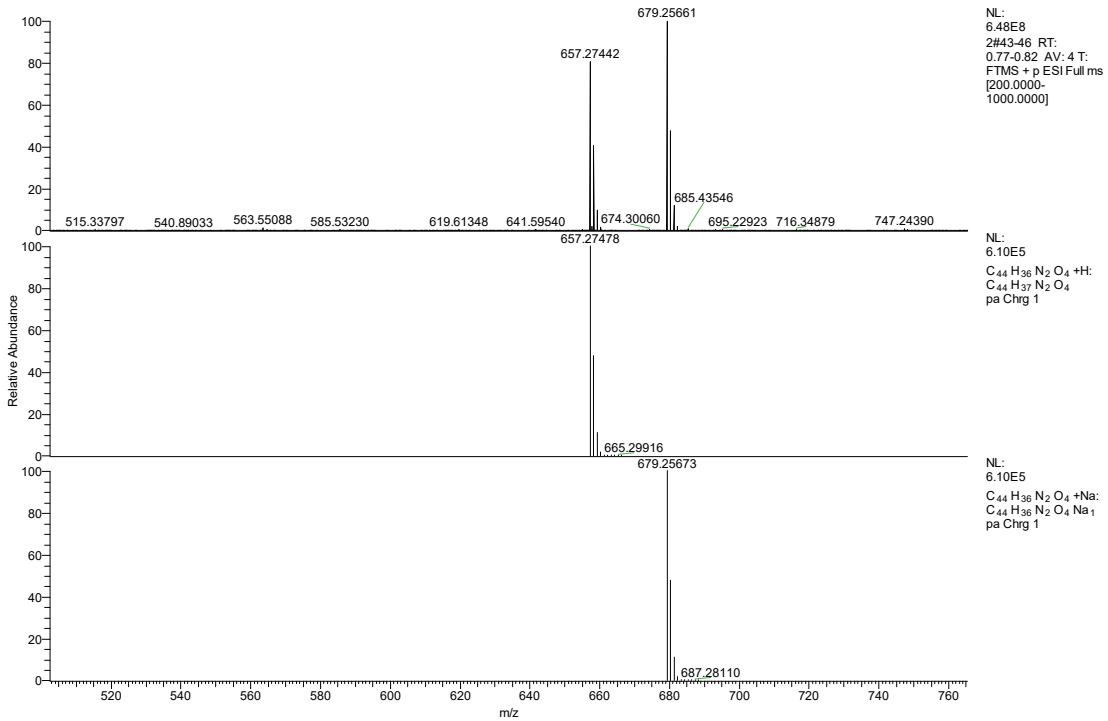

Fig. S10. ESI-MS spectrum of DDBA at room temperature.

HR-MS (ESI, m/z): $[M+H]^+$ calcd for $C_{44}H_{37}N_2O_4$, 657.27478, found 657.27442. $[M+Na]^+$ calcd for $C_{44}H_{36}N_2O_4Na$, 679.25673, found 679.25661.

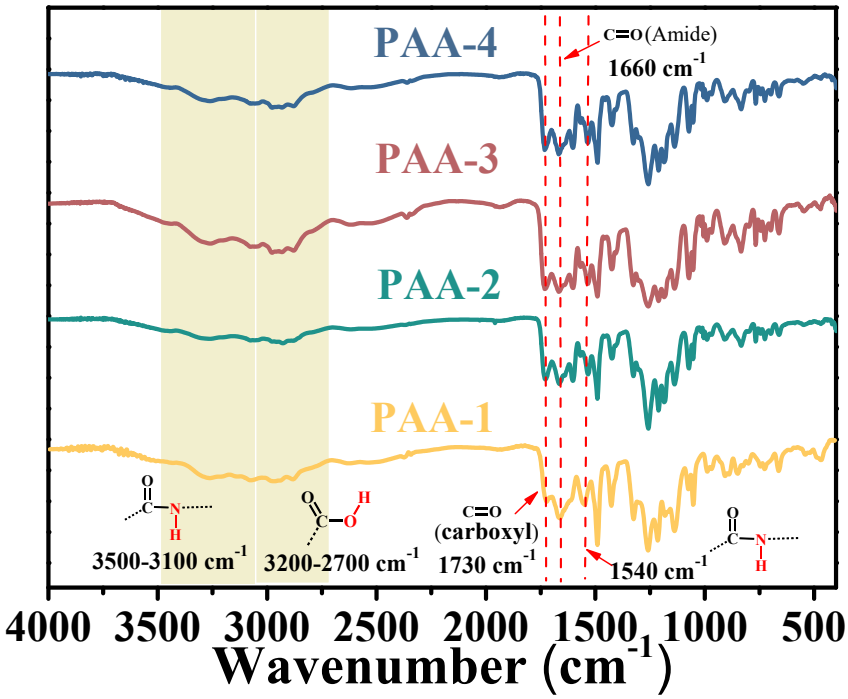

Fig. S11. FT-IR spectra of polyamide acid (PAA).

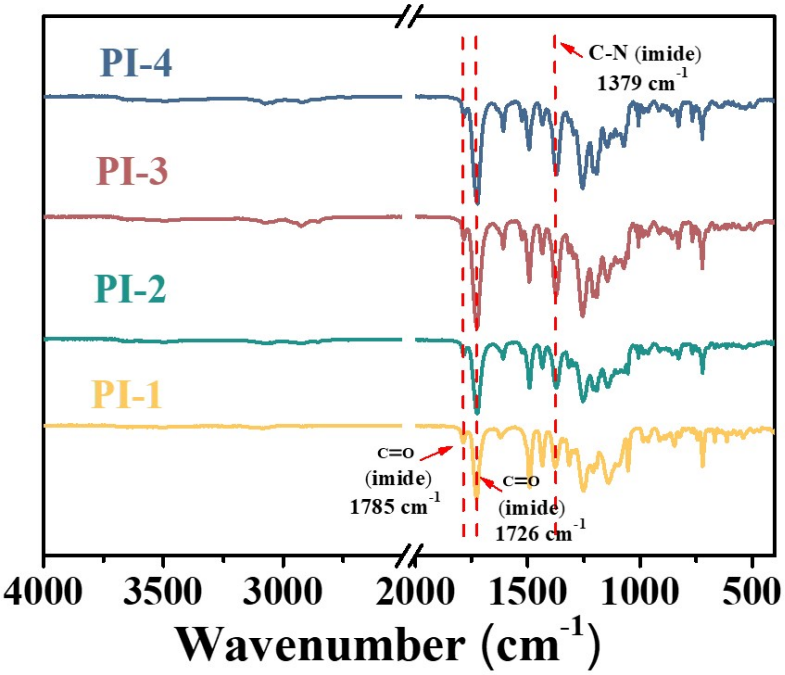

Fig. S12. FT-IR spectra of polyimides (PI).

As shown in the FT-IR spectra (**Fig. S11**), the amide carbonyl stretching vibration at approximately 1660 cm^{-1}, the NH variable angle vibration at approximately 1540 cm^{-1}, and the broad peak corresponding to the NH stretching vibration at approximately 3200 cm^{-1} were observed, indicative of the presence of an amide group. Furthermore, the carboxyl group characteristic of the aromatic acid was discernible at 1730 cm^{-1}, which represents the C=O stretching vibration of the hydrogen bond. The OH stretching vibration, which was also part of the hydrogen bonding network, was observed in the range of 2700 to 3200 cm^{-1}. These spectroscopic features collectively confirm the successful synthesis and structural integrity of the polyamide acid (PAA). The resulting PAAs were then chemically imidized by mixing acetic anhydride with pyridine. As illustrated in the FT-IR spectra of polyimides (**Fig. S12**), the characteristic peaks of the above PAA were no longer discernible, while the imide carbonyl absorption at around 1785 cm^{-1} (asymmetric) and 1726 cm^{-1} (symmetric), and the C–N adsorption peaks at around 1379 cm^{-1} were observed, indicating that the PI structures were successfully synthesized.

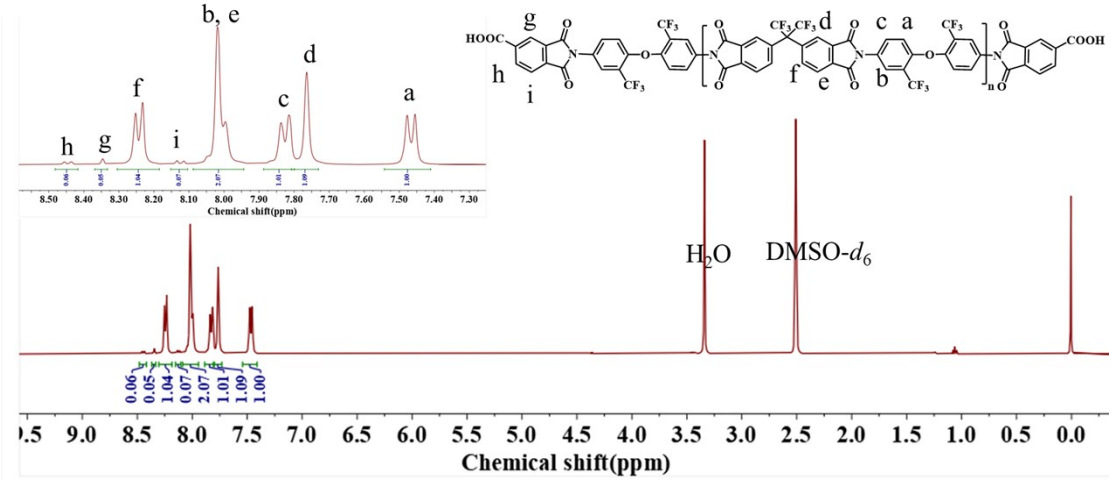

Fig. S13. ^{1}H NMR spectrum of PI-1 in DMSO-d_6.

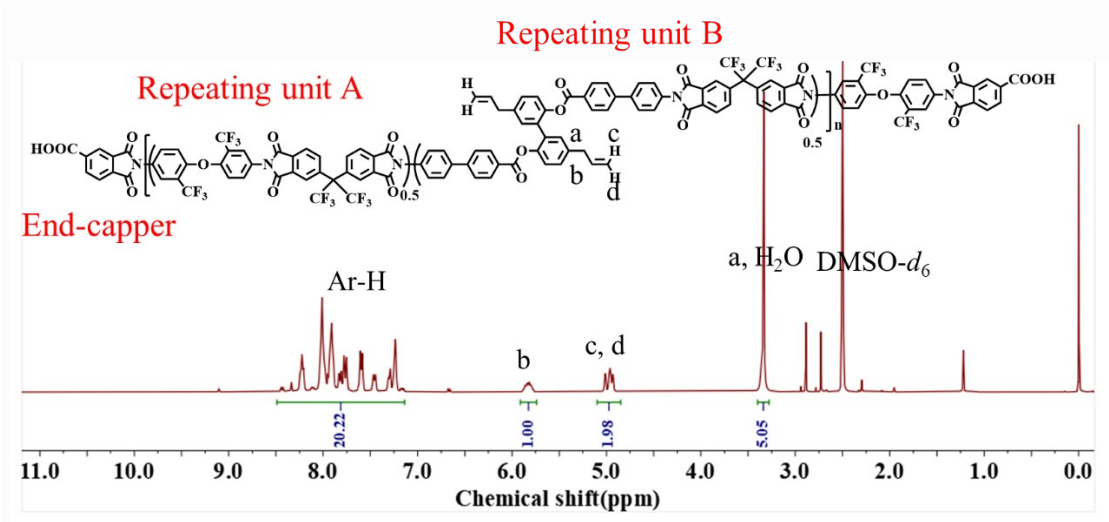

Fig. S14. ^{1}H NMR spectrum of PI-2 in DMSO-d_6.

The peaks assigned to the protons in the allyl group (a, b, c, d: 3.34, 5.83, 4.95, 5.00 ppm), and the protons in the aromatic rings in the range of 7.23–8.45 ppm were all observed in the ^{1}H NMR spectrum (**Fig S14**). Random-sequence PI-2 with a number-average molecular weight (M_n) of 2.81 $\times 10^4$ g·mol^{-1} consisted of multiple repeating units A and B, which was end-capped with trimellitic anhydride. When the molar feed ratio of DDBA and 6FODA is 1:1, the number of repeating units A and B is equal. In this case, the theoretical molar ratio of the number of the protons (b) of the allyl group to that of the aromatic ring on the repeat unit (A+B) is 1:20. It is worth noting that the end-cappers present a relatively small molar ratio to the total polyimide chains, of which the molar ratio of the aromatic protons to that of the allyl group is small. As described in the review, the molar ratio of the protons (b) of the allyl group to that of the aromatic ring (Ar-H) is reasonable. The above result confirmed the expected chemical structure of **PI-2.**

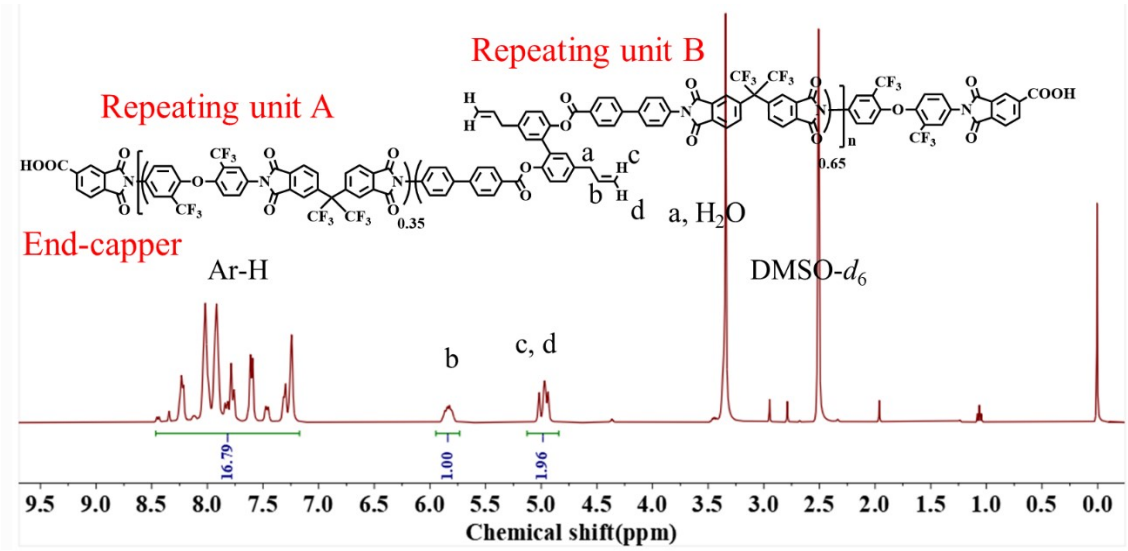

Fig. S15. ^{1}H NMR spectrum of PI-3 in DMSO-d_6.

When the molar feed ratio of DDBA and 6FODA is 0.65: 0.35, the theoretical molar ratio of the number of the protons (b) of the allyl group to that of the aromatic ring on the repeat unit (A+B) is 1:16.

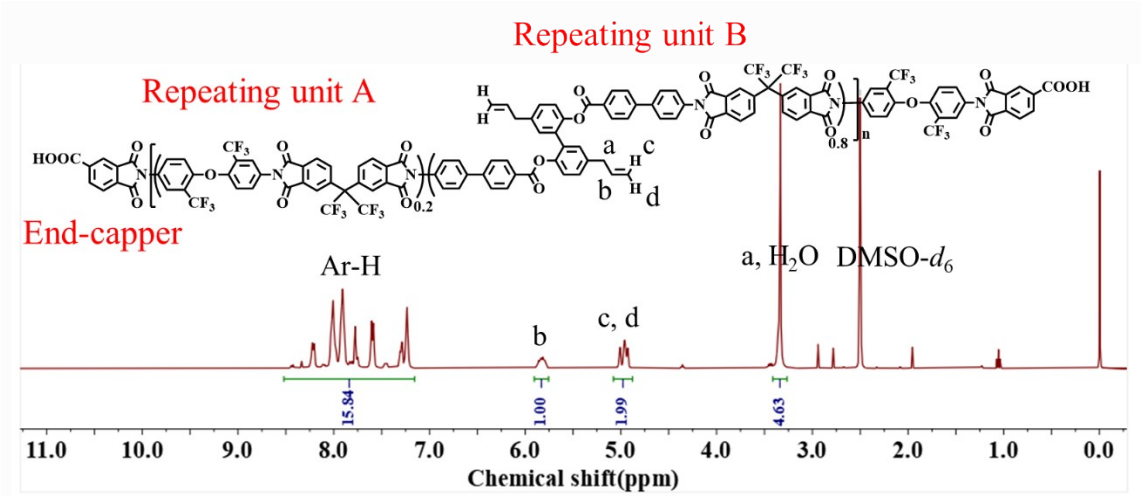

Fig. S16. ^{1}H NMR spectrum of PI-4 in DMSO-d_6.

When the molar feed ratio of DDBA and 6FODA is 0.8: 0.2, the theoretical molar ratio of the number of the protons (b) of the allyl group to that of the aromatic ring on the repeat unit (A+B) is 1:15.5.

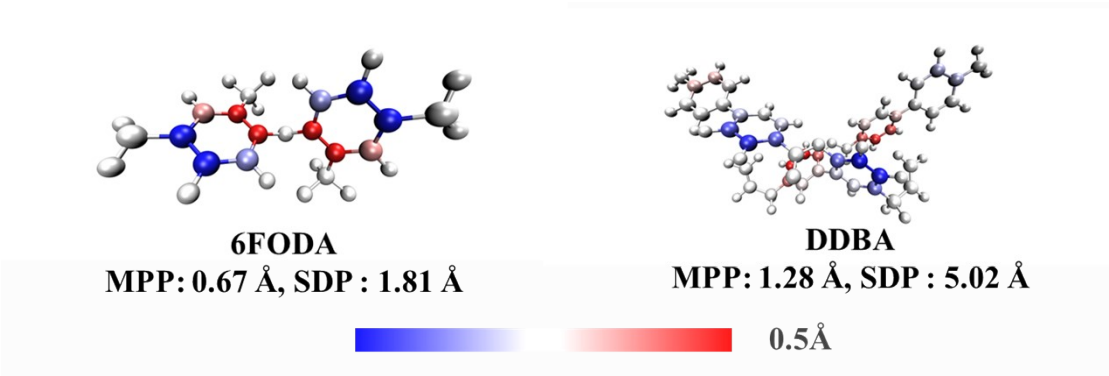

Fig. S17. MPP and SDP (in Å) calculated for all atoms of 6FODA and DDBA. Atoms are colored according to d^s values. The degree of blueness (redness) is directly proportional to the distance of the atom below (above) the overall fitting plane.

Given that DDBA is a fluorine-free diamine monomer, it is essential to investigate its molecular planarity prior to conducting a dissolution experiment on synthetic polyimide resins. In accordance methodology previously reported for quantifying planarity[3, 6], the molecular planarity parameters (MPP) and the span of deviation from plane (SDP) of 6FODA and DDBA were calculated, respectively. As illustrated in **Fig S17**, the MPP value of DDBA (1.28 Å) is much greater than that of 6FODA (0.67 Å), demonstrating that DDBA displayed more non-coplanar characteristics than 6FODA. Concurrently, DDBA exhibited elevated SDP values in comparison to 6FODA, indicating that the red and blue colored atoms in DDBA molecules deviate to a greater extent from the overall fitting plane.

Table S1 Solubility, molecular weight, intrinsic viscosity, and transparency of polyimide resins.

	Solvent[a]							Molecular weight			η^b	$\lambda_0{}^c$	AVT[d]
	NMP	DMAc	THF	DCM	NVP	PGEMA	EA	M_n ($\times10^4$ g·mol^{-1})	M_w ($\times10^4$ g·mol^{-1})	PDI	(dL·g^{-1})	(nm)	(%)
PI-1	+	+	+	+	+	+	+	2.81	3.72	1.32	0.35	323	93.0
PI-2	+	+	+	+	+	+	+	2.81	3.76	1.34	0.25	342	89.5
PI-3	+	+	+	+	+	+	+	2.77	3.67	1.32	0.25	342	89.2
PI-4	+	+	+	+	+	+-	-	3.02	4.04	1.34	-	-	-

[a] The solubility was measured with 10 mg samples in 1 mL solvent for 24 h; +: soluble at room temperature; +-: partially soluble on heating; -: insoluble even on heating. NMP: *N*-Methyl pyrrolidone; DMAc: *N, N*-dimethylacetamide; THF: tetrahydrofuran; DCM: dichloromethane; NVP: *N*-vinyl-2-Pyrrolidinone; PGEMA: 2-acetoxy-1-methoxypropane; EA: ethyl acetate. [b] The intrinsic viscosity (η)

was measured with an Ostwald viscometer in PGEMA solvent at 30 °C. [c] Cut-off wavelength. [d] Average visible light transmittance (400-780 nm) of PI films with 9 ±1 μm thickness.

The η of the PIs with similar molecular weight decreased as part of the replacement of 6FODA by DDBA, which may be attributed to the steric hindrance of DDBA to force the rings out of plane. In this case, the eventual twist in the backbones of the PIs weakened the intermolecular interactions to exhibit a relatively low viscosity.

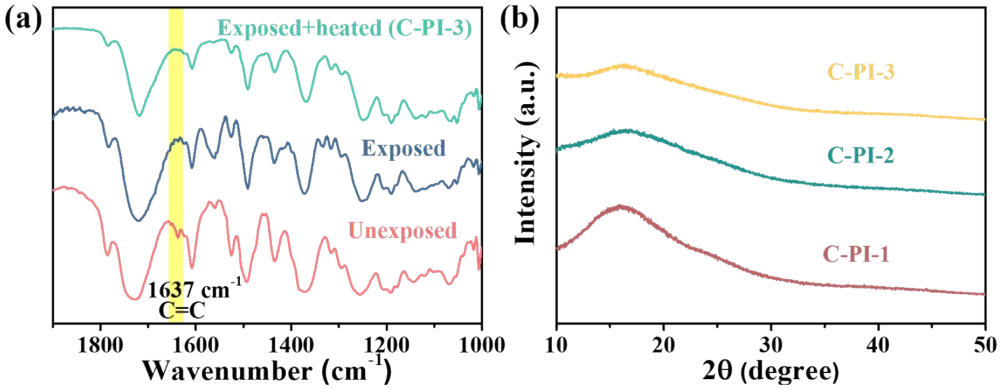

Fig. S18. (a) The enlarged regions of the FT-IR spectra of C-PI-3 under different processing conditions, (b) X-Ray diffraction profiles of the cured PSPI films.

Table S2 Results of the cured PSPI films in chemical resistance experiment[a, b7].

	C-PI-1	C-PI-2	C-PI-3
PGEMA	bad	good	good
NMP	bad	good	good
Acetone	bad	good	good
30% H_2SO_4	good	good	good
30% HNO_3	good	good	good
30% H_2O_2	good	good	good

[a] Condition: 25.8 °C, 15 min. [b] The film thickness change of less than 3% before and after the chemical resistance experiment is considered good, otherwise it is bad.

Despite the absence of cross-linking sites in **PI-1**, the cross-linking structure of TMTM and TAC protected **PI-1** from organic solvent etching[8].

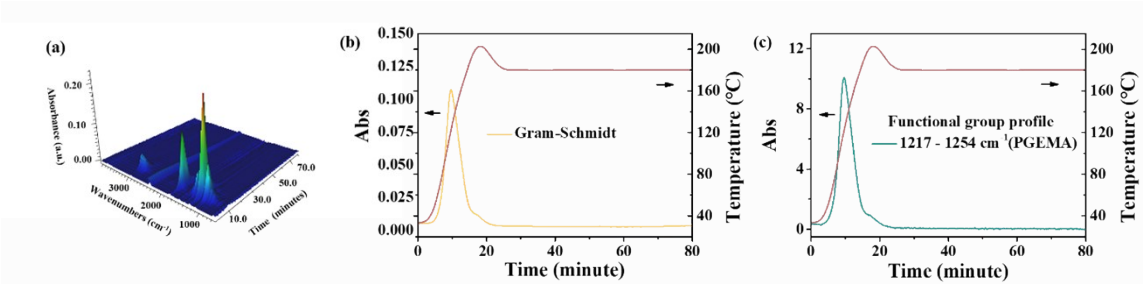

Fig. S19. Three-dimensional FT-IR spectra, Gram-Schmidt (GS) curves and functional group profiles (FGP) of UV-exposed wet film of C-PI-3 used PGEMA as solvent.

The GS curve is a quantitative measure of total infrared absorption, showing the change in the concentration of escaping gases over time. The FGP is often used to express the relationship between a specific wavenumber in the gas escaping during an experiment and the measurement time or temperature. The region between 1217 and 1254 cm^{-1} is a specific absorption of the solvent PGEMA. It was obvious that this region was not disturbed by other absorption peaks, so the wavenumber of this peak can be used as a basis for FGP curves to assess the escape of PGEMA with increasing temperature. The FGP curves were very close to the GS curves of the UV-exposed wet film (**C-PI-3**). In addition to the characteristic absorption of the solvent, no excess absorption peaks were detected in the differential spectrum, indicating that only solvent volatilized during the hardbake process.

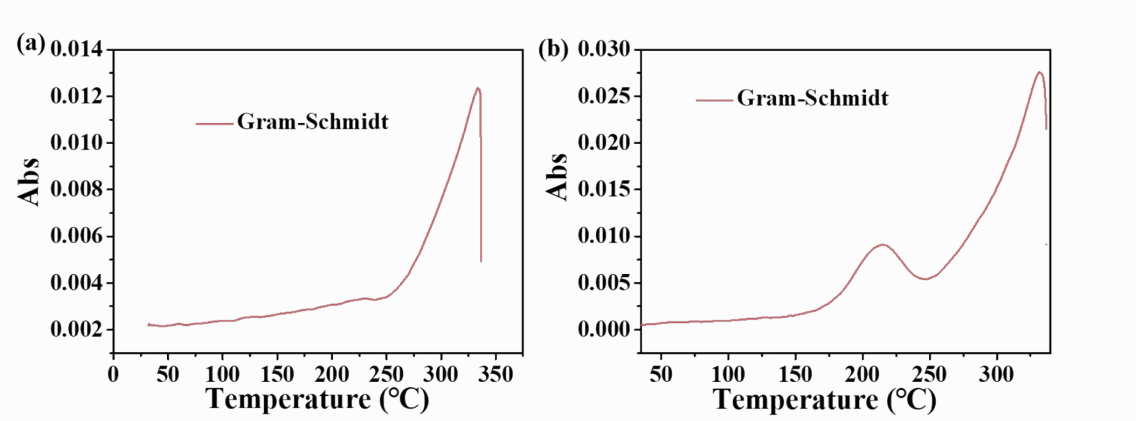

Fig. S20. Gram-Schmidt (GS) curves of escaping gas during heating processes: the C-PI-3 films used (a) PGEMA, (b) NMP as solvent after curing at 180 °C for 1 h.

Table S3 The excitation energy and oscillator strength of the model compounds.

Index	MC-6FODA		MC-DDBA	
	Excitation energy(nm)	Oscillator strength	Excitation energy(nm)	Oscillator strength
1	398.84257	0.0096	425.55071	0.0150
2	396.86374	0.0114	425.33173	0.0135
3	395.98914	0.0032	417.87732	0.0052
4	394.15120	0.0023	417.14622	0.0015
5	361.01738	0.0004	377.90844	0.0002
6	359.30159	0.0006	377.40229	0.0013
7	354.11916	0.0000	377.28744	0.0001
8	351.99784	0.0000	376.73716	0.0000
9	343.41800	0.0009	375.17536	0.0000
10	342.15752	0.0008	375.08456	0.0000

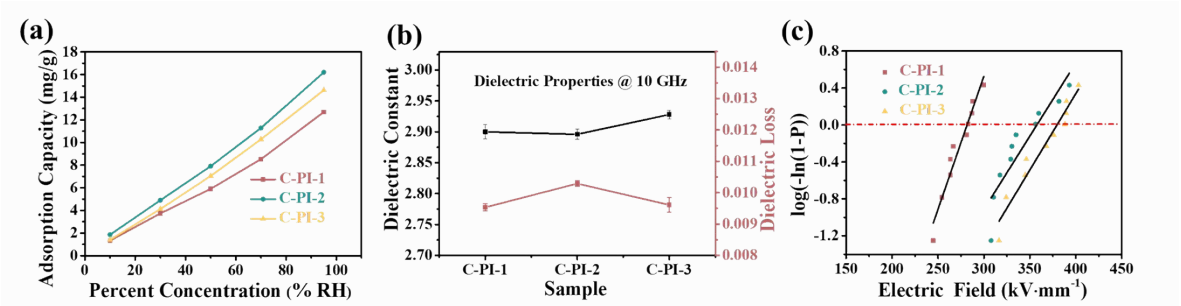

Fig. S21. (a) Water adsorption at different humidity concentrations ("gravimetric method"), (b) dielectric properties at 50 % RH, 25 ℃ and (c) breakdown strength by Weibull distribution of the cured PSPI films.

As shown in **Fig. S21a**, the water adsorption of cured PSPI films gradually increased with increasing water vapor concentration. Among the cured PI resins, **C-PI-1** with the highest content of hydrophobic fluorine monomers was endowed with the lowest value of water adsorption. In this case, the water absorption value of **C-PI-3** should be higher than that of **C-PI-2**. But the opposite is true, probably as the higher cross-linking density of **C-PI-3** played a positive role in hindering water molecules from penetrating and diffusing into the resins[9]. That means that the difference in water adsorption is related to both the chemical and aggregated structure of the cured PSPI films.

Due to the low water absorption, the cured PSPI films also exhibited satisfactory dielectric properties. In the field of advanced packaging, signal propagation in the conductive traces is significantly correlated with the dielectric properties of dielectric films. A lower dielectric constant (D_k) improves transmission speed, while a lower D_f ensures signal integrity[10]. The dielectric properties of the cured PSPI films were presented in **Fig. S21b.** The D_f values of the cured PI films at 10 GHz (50 %RH, 25℃) was found to be 0.0095 - 0.0103, which was mainly determined by its water adsorption, followed by the structure of PI[11, 12]. It is worth confirming that such low D_f values at 10 GHz of cured PI films in this study were excellent with the existence of components for photo lithography after the low-temperature curing process. Furthermore, the D_k value of C-PI-3 (**2.93**) was slightly higher than those of **C-PI-1** (2.90) and **C-PI-2** (2.90). The lower D_k value of C-PI-1 was mainly attributed to a relatively large number of low-polarity fluorine atoms. However, the introduction of DDBA increased the intermolecular free volume for **C-PI**-2 and **C-PI-3**. The movement of the molecular chain was restricted and the non-coplanar molecular configuration was induced after cross-linking reactions between the allyl side groups and curing agents. The above factors were also conducive to reduce the D_k values for **C-PI-2** and **C-PI-3**, which was probably able to compensate for the influence of the fluorine content[10].

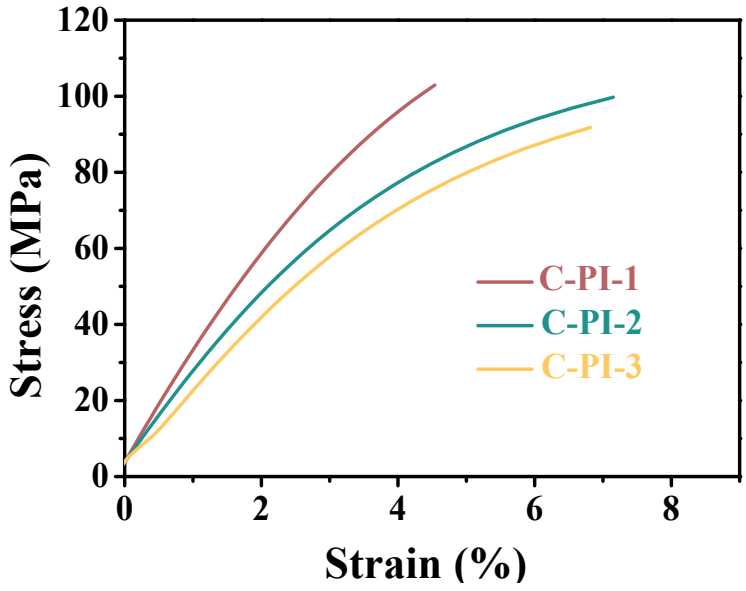

Fig. S22. Stress- strain curves of the cured PSPI films.

Table S4 The maximum curing temperature and the maximum patterning resolution of the reported photosensitive polyimides.

Sample name	Maximum Curing temperature (°C)	Maximum resolution (μm)	Ref
FPI-7	250	20	[13]
Polymer 20e	250	10	[14]
PSPI-2	350	10	[15]
n-PSPI-2	350	7	[16]
n-LTPI-IMZ-2.0	230	5	[17]
PI(SDA-ODPA)	200	4	[18]
C-PI-3	180	5	In this work

References

1. A. Larsen, K. Hansen, P. Sommer-Larsen, O. Hassager, A. Bach, S. Ndoni and M. Jørgensen, *Macromolecule*, 2003, **36**, 10063-10070.
2. L. Dissado, J. Fothergill, S. Wolfe and R. Hill, *IEEE Trans. Dielectr. Electr. Insul.*, 1984, **E1-19**, 227-233.

3. T. Lu and F. Chen, *J. Comput. Chem.*, 2011, **33**, 580-592.
4. M. Frisch, G. Trucks, H. Schlegel, G. Scuseria, M. Robb, J. Cheeseman, G. Scalmani, V. Barone, G. Petersson and H. Nakatsuji, 2016.
5. M. J. Abraham, T. Murtola, R. Schulz, S. Páll, J. C. Smith, B. Hess and E. Lindahl, *SoftwareX*, 2015, **1-2**, 19-25.
6. T. Lu, *J. Mol. Model.*, 2021, **27**, 263.
7. Y. Shoji, Y. Koyama, Y. Masuda, K. Hashimoto, K. Isobe and R. Okuda, *J. Photopolym. Sci. Technol.*, 2016, **29**, 277-282.
8. H. C. Tien, X. Li, C. J. Liu, Y. Li, M. He and W. Y. Lee, *Adv. Funct. Mater.*, 2023, **33**, 2211108.
9. K. Guo, J. Zhan, S. Qi, G. Tian and D. Wu, *Eur. Polym. J.*, 2024, **205**, 112723.
10. Y. Li, G. Sun, Y. Zhou, G. Liu, J. Wang and S. Han, *Prog. Org. Coat.*, 2022, **172**, 107103.
11. R. Bei, K. Chen, Q. Liu, Y. He, C. Li, H. Huang, Q. Guo, Z. Chi, J. Xu, Z. Chen, S. Liu and Y. Zhang, *Macromolecules*, 2024, **57**, 2142-2153.
12. R. Bei, K. Chen, Y. He, C. Li, Z. Chi, S. Liu, J. Xu and Y. Zhang, *J. Mater. Chem. C*, 2023, **11**, 10274-10281.
13. Y. Gao, H. Wang, J. Jia, Z. Pan, X. Ren, X. Zhi, Y. Zhang, X. Du, X. Wang and J. Liu, *Polymers-Basel*, 2022, **14**, 3733.
14. K.-H. Kim, S. Jang and F. W. Harris, *Macromolecules*, 2001, **34**, 8925-8933.
15. X. W. Lai, J. L. Zhang, Z. X. Yang, S. Huang, J. H. Li, G. P. Zhang and R. Sun, *Mater. Today Commun.*, 2023, **37**, 107316.
16. J.-x. Ma, L.-l. Yuan, S.-n. Fan, L.-z. Wang, B. Jia, H.-x. Yang and S.-y. Yang, *Eur. Polym. J.*, 2023, **192**, 112071.
17. S. N. Fan, L. L. Yuan, L. Z. Wang, B. Jia, J. X. Ma, H. X. Yang and S. Y. Yang, *Polymers-Basel*, 2023, **15**, 973.
18. E. C. Chang, L. Y. Tseng, Y. Liu, C. K. Chen, C. C. Kuo, M. Ueda, Y. C. Lin and W. C. Chen, *J. Polym. Sci.*, 2023, **61**, 2122-2132.